Measurement of Multisite Oxidation Kinetics Reveals an Active Site Conformational Change in Spo0F as a Result of Protein Oxidation†

Joshua S. Sharp,‡ Daniel M. Sullivan,§ John Cavanagh,*,§ and Kenneth B. Tomer‡

Laboratory of Structural Biology, National Institute of Environmental Health Sciences, National Institutes of Health, Department of Health and Human Services, Research Triangle Park, North Carolina 27709, and Department of Molecular and Structural Biochemistry, North Carolina State University, Raleigh, North Carolina 27695

Received March 9, 2006; Revised Manuscript Received April 18, 2006

ABSTRACT: When most proteins undergo oxidative damage, they yield a variety of products containing oxidative damage at a large number of sites, most of which are modified substoichiometrically. The resulting complex mixture of products is not amenable to high-resolution structural analyses. The previous methods of structural analysis have relied upon either very generalized structural analyses such as circular dichroism or the creation of a battery of mutants to try to isolate single-residue damage effects. We present a methodology using mass spectrometry to measure the kinetics of oxidation at many sites simultaneously. Previous studies have shown that these kinetics are determined by the chemical nature of the damage site and by the accessibility of that site to the radical. By measuring deviations in the rate of oxidation from the expected pseudo-zero-order kinetics, we can detect and characterize local structural changes due to the oxidative damage. We demonstrate the application of this new technique to the Spo0F protein, a regulator of sporulation in *Bacillus subtilis*. Circular dichroism studies suggest a partial loss of helical structure of Spo0F as a result of oxidative damage. We report that oxidation causes a three-stage conformational change in Spo0F. Furthermore, we find the dramatic structural changes affect only the region surrounding the active site, while the remainder of the structure remains relatively unperturbed. Finally, we are able to determine that the specific oxidation event that triggers the conformational change at the active site of Spo0F occurs at Met81, a partially conserved methionine in the CheY superfamily.

Oxidative stress is a condition in which a cell's reductive capacity is unable to cope with the accumulation of intracellular reactive oxygen species. Such a circumstance can arise from aerobic metabolic processes, exposure to metals and redox-active chemicals, and the activity of ionizing radiation (*1*). It is generally accepted that challenge by a number of stresses, including oxidative stress, decreases the proportion of cells in a culture undergoing sporulation. Recent work indicates that shear stress leads to a 20-fold reduction in the ability of cells to sporulate due to the generation of reactive oxygen species (ROS),[1] specifically superoxide radical derivatives, within the cell. It was further found that induction of oxidative stress through the addition of exogenous hypochlorus acid or hydrogen peroxide also caused a similar inhibition of sporulation, and reduction of the intracellular ROS rescues sporulation (*2*).

To study the attenuation of the sporulation cycle by oxidative stress, we are initially investigating proteins involved in the developmental pathway prior to engulfment of the forespore. Following this stage (termed stage 3), the cells are fully committed to sporulation (*3*). Previous work has implicated the stage 0 proteins in the temporal regulation of a number of oxidative stress proteins, including the vegetative catalase encoded by the gene *kat-19* (*4*, *5*). Accordingly, a particularly appealing target for the downregulation of sporulation is the stage 0 signal transduction pathway that is responsible for its initiation. The initiation of sporulation in *Bacillus subtilis* is tightly regulated by an exquisite signaling mechanism termed the multicomponent phosphorelay pathway (*6*). In response to distinct environmental signals arising from nutritive deprivation and cell density, the primary sensor kinase KinA autophosphorylates on a conserved histidine. KinA transfers this phosphoryl group to a conserved Asp residue in the conserved Asp pocket of the single-domain response regulator protein, Spo0F. The phosphoryl group is subsequently transferred from Spo0F to a conserved histidine on the phosphotransferase, Spo0B, and ultimately to the response regulator domain of the "master switch" of sporulation, Spo0A. The phosphorylation of Spo0A serves to activate the protein. Activated Spo0A-P is a transcription factor, initiating the cascade of gene activation required for the proper formation of a viable spore (*7*). Considering that oxidative stress leads to a downregulation of sporulation, it is reasonable to presume that a mechanism may exist by which intracellular reactive oxygen species act upon components of the phosphorelay pathway in a negative fashion.

† This research was supported in part by the Intramural Research Program of the National Institutes of Health, National Institute of Environmental Health Sciences.

* To whom correspondence should be addressed.

‡ National Institutes of Health.

§ North Carolina State University.

[1] Abbreviations: ROS, reactive oxygen species; MS, mass spectrometry; Q-TOF, quadrupole time-of-flight; MS/MS, tandem mass spectrometry; fwhm, full width at half-maximum; CD, circular dichroism.

10.1021/bi060470r CCC: $33.50
Published on Web 05/03/2006

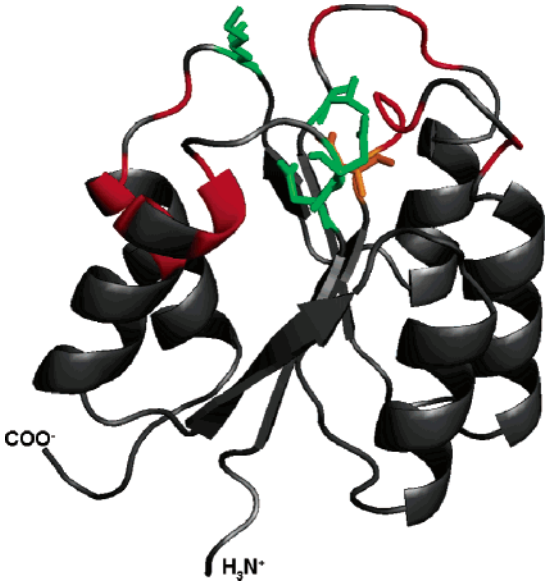

FIGURE 1: Ribbon illustration of the average NMR solution structure of Spo0F. The phosphorylation site, Asp54, is colored orange, with the sites essential for phosphorylation and activity colored green (Asp10, Asp11, Thr82, and Lys104). Regions of Spo0F that have been shown by Ala mutagenesis to impact the function of Spo0F are colored red on the NMR structure of Spo0F.

This study focuses upon delineating the effects of oxidative damage to response regulator Spo0F, the first cytosolic sporulation protein downstream of the membrane-bound histidine kinase. We have previously characterized the high-resolution NMR structure and dynamics of Spo0F, making it an ideal candidate for this study (*8*−*10*). Spo0F is a 124-residue, α5/β5 single-domain protein in which the helices are arranged around a central parallel β-sheet core, helices 1 and 5 on one face of the β-sheet and helices 2−4 on the other face (see Figure 1). At the "bottom" of the structure, removed from the phosphorylation site, are short α−β loops connecting elements of secondary structure (e.g., α1−β2, α2−β3, etc.). As with all other response regulator proteins, Spo0F has a conserved aspartic acid pocket at the "top" of the protein composed of Asp residues 10, 11, and 54, the residue phosphorylated by KinA. This Asp pocket is surrounded by five functionally critical β−α loops (β1−α1 to β5−α5). Residues making up the β−α loops as well as a subset of helical surfaces are essential for the activity of Spo0F, directing the proper interactions with KinA, the phosphotransferase Spo0B, and the phosphatase RapB (*11*−*13*). Additionally, metal binding studies have indicated a distinct role of the β−α loops in binding divalent Mg^{2+}, which is required for phosphorylation. Furthermore, backbone dynamic studies via NMR have revealed the key role of the β−α loop regions in an intramolecular communications network within Spo0F responsible for transmitting the state of phosphorylation throughout the protein (*8*, *9*). Indeed, all the known molecular recognition and interaction properties of Spo0F are contained within the β−α loops and the N-terminal end of the α1 helix which is contiguous with the β1−α1 loop. Consequently, any impacts in this region would significantly impede function.

Protein oxidative surface mapping has been used previously to describe the topology of a number of proteins in solution (*14*−*17*). The rate of oxidation has been shown to be largely dependent on a combination of the inherent reactivity of the oxidized side chain and the solvent accessibility of that side chain (*14*−*19*), with pseudo-first-order rate constants ranging across 3 orders of magnitude. Sulfur-containing and aromatic amino acids are the most susceptible to oxidation (5.0×10^9 to 3.4×10^{10} M^{-1} s^{-1}), followed by the various aliphatic, acidic, basic, and alcohol-containing residues (2.3×10^8 to 3.5×10^9 M^{-1} s^{-1}), with Ala, Asn, Asp, and the backbone α-carbon the least reactive ($1.7-7.7 \times 10^7$ M^{-1} s^{-1}) (*20*). The most common product of amino acid side chain oxidation is the addition of one oxygen; however, some amino acids have major oxidation pathways that result in other characteristic mass shifts (*21*, *22*). As the rate of amino acid oxidation depends on the inherent reactivity and solvent accessibility, and the inherent reactivities of the amino acids are known, a careful measurement of the rate of oxidation at a particular site can be used to detail conformational changes that alter the solvent accessibility of that site. In this study, we present a comprehensive analysis of the structural effects of oxidative damage on the response regulator Spo0F using quadrupole time-of-flight mass spectrometry (Q-TOF MS). We compare our results with those generated using circular dichroism, one of the standard analytical techniques for studying structural changes due to oxidative damage. We show that our technique not only agrees with the data generated by circular dichroism but also is able to provide much more detail about both the nature of the structural changes and the cause of the most dramatic conformational shift detected. We were able to generate these data using only small amounts of protein in one experiment, with no mutagenesis or other modification of the analyte required. This technique represents a significant advance in the methodology for studying structural effects of oxidative damage to proteins.

Our previous NMR structure and dynamics studies show that the β−α loops have some conformational flexibility on the micro- to millisecond time scale (*8*, *10*). Nevertheless, these loops cluster at the top of the protein. In this study, we show conclusively that, in response to mild oxidation, a conformational change at Met81 triggers a localized conformational change that relaxes and opens up the cluster of β−α loops around the phosphorylation site. This conformational event severely affects the structure of the regions previously identified as being necessary for Spo0F function and, therefore, would inhibit the organism's ability to initiate sporulation.

EXPERIMENTAL PROCEDURES

Spo0F Sample Preparation. Spo0F was expressed and purified as previously described (*23*). Spo0F was diluted to a concentration of 10 or 20 μM in 2 mM ammonium bicarbonate (pH 6.8). No attempts were made to degas the solution at any point during handling; therefore, the sample should be considered air-saturated. Bovine catalase was added to a final concentration of 10 nM tetramer to eliminate hydrogen peroxide generated during radiolysis and prevent secondary oxidation (especially of methionine) (*24*). Aliquots of 100 μL were placed in 500 μL polypropylene tubes and exposed to γ-irradiation in a ^{137}Cs dual source γ-irradiator at a dosage rate of 0.0236 kGy/min for varying amounts of time at 23 °C. The samples were rotated on a turntable during exposure at a rate of ~60 rpm to ensure equal radiation

exposure for all samples. The 20 μM Spo0F samples were used for circular dichroism spectroscopy. The 10 μM Spo0F samples were heated to 85 °C for 1 h to denature the protein; 20 μg of lyophilized sequencing-grade modified trypsin (Promega, Madison, WI) was dissolved in 40 μL of trypsin resuspension buffer. To each irradiated Spo0F aliquot was added 2 μL of resuspended trypsin (a total of 1 μg), and the samples were placed in a rotating incubator at 37 °C for 48 h.

Circular Dichroism Spectroscopy. Samples were analyzed using a Jasco J-810 circular dichroism spectrophotometer (Jasco, Easton, MD) in a quartz cell with a path length of 1 mm. All spectra were obtained in quadruplicate, with the four signals averaged together for final output. The CD spectrum of 2 mM ammonium bicarbonate was then subtracted from all Spo0F spectra to eliminate the signal from the buffer, and the units were converted into molar ellipticity.

Nanoelectrospray Quadrupole Time-of-Flight Mass Spectrometry. Irradiated Spo0F was mixed 50:50 with acetonitrile with 0.2% formic acid to a final concentration of 4.9 μM irradiated Spo0F and injected directly into a hybrid quadrupole time-of-flight Micromass Q-TOF Ultima Global mass spectrometer using a Waters nanoflow electrospray source. Typical nanoelectrospray parameters were used for the MS analyses (3200 V capillary potential, 100 V cone potential, and 10 V collision cell potential) and the MS/MS analyses (3200 V capillary potential, 100 V cone potential, and 15 V collision cell potential). The signal was accumulated for 9 min for each sample, split into three separate data sets of with accumulation for 3 min each. These data sets were independently averaged. A typical mass resolution of ~12000 fwhm was achieved, with a typical mass accuracy of ~400 ppm using external calibration only. When insufficient signal was present in the three data sets to generate three values, all three data sets were combined and averaged, and only a single value was used. Peptide identities were assigned by high-resolution mass measurement and, when possible, MS/MS analysis. The resulting mass spectra were used to determine the kinetics of oxidation by measuring the signal intensity of the unoxidized version of each peptide and comparing the signal intensity with that of each of the various oxidized versions. The average number of oxidations per peptide was generated by the function $R = ([M+O] + 2[M+2O] ...)/([M] + [M+O] + [M+2O] ...)$, where [M] is the ion abundance of the unmodified peptide, [M+O] is the abundance of the peptide plus 16 Da, [M+2O] is the abundance of the peptide plus 32 Da, etc. The rate of oxidation was determined by dividing the average number of oxidations per peptide by the radiation dosage in kilograys. When multiple charge states could be measured, the charge state that exhibited the lowest standard deviation in the amount of oxidation across all irradiation dosages was used for analysis to minimize experimental error. When multiple overlapping peptides were detected, the peptide with the highest signal level was used for analysis (usually representing the completed digestion product).

Solvent Accessibility Analysis. All solvent accessibility analyses were performed using GETAREA version 1.1 (http://www.scsb.utmb.edu/cgi-bin/get_a_form.tcl) using the 2FSP structure as a template, with the solvent accessibility calculated for each individual atom.

RESULTS

We initially examined the structural effects of oxidative damage on Spo0F using circular dichroism (CD) spectroscopy. As circular dichroism is a traditional structural analysis tool for oxidative damage, these results can be used as a standard for comparison of our own results from oxidative damage kinetics analysis. The results and analysis of CD spectroscopy are given as Supporting Information. These data are consistent with a model in which oxidative damage leads to partial conversion of α-helix to random coil, with the largest transitions occurring between 0.472 and 0.708 kGy, and 0.944 and 1.180 kGy exposure. However, even if this model is correct, it does not reveal which portions of the helical structure are converting to random coil. To understand the mechanism of protein oxidative damage at the molecular level, a more thorough probe of structural changes must be developed.

Under the slow reaction conditions used here, the rate of product formation is determined by the rate of hydroxyl radical reaction with the oxidation target, which is the irreversible step in the reaction (*21*). Hydroxyl radical attack typically occurs via second-order kinetics (*20*). In these experiments, the initial concentration of protein is much greater than the concentration of hydroxyl radical; furthermore, the hydroxyl radical is generated by continuous radiolysis of water, leading to a constant concentration of hydroxyl radical throughout the course of the experiment. Under these pseudo-zero-order conditions, the rate of oxidation of an amino acid target will be constant, as long as the concentration of the unmodified target is much greater than the concentration of the hydroxyl radical. This constant rate will be determined by two factors: the inherent chemical reactivity of the target and the accessibility of the target to the radical (*14*−*19*). As the chemical reactivity of the target will remain essentially unchanged, by measuring the apparent rate of oxidation and plotting it as a function of radiation dose, we can measure changes in solvent accessibility as a function of oxidative damage. The presence of such changes in the apparent rate of oxidation would indicate a conformational change affecting the solvent accessibility of the measured oxidation target. In this report, the kinetics of oxidation are provided as oxidation events per molecule per kGy of radiation exposure. This unorthodox nomenclature is used so that future experiments that may be performed using different concentrations of protein and different intensities of radiation may be easily compared.

We examined the rates of oxidation for 11 different regions of Spo0F simultaneously, containing a minimum of 14 discrete oxidation sites. A total of 92% sequence coverage was obtained for the protein by analysis using direct infusion nanospray into a hybrid quadrupole time-of-flight mass spectrometer, with the only regions of missing data consisting of the first five residues of the N-terminus, the last two residues of the C-terminus, and a tripeptide from residue 68 to 70. The native structure of Spo0F has been determined, both by X-ray crystallography and in solution by NMR spectroscopy (*10*, *25*). Therefore, we can examine the kinetics of oxidation of each residue in the context of the native structure and determine which portions of the native structure (if any) are undergoing changes in conformation as a result of oxidative damage. The kinetics of oxidation for each

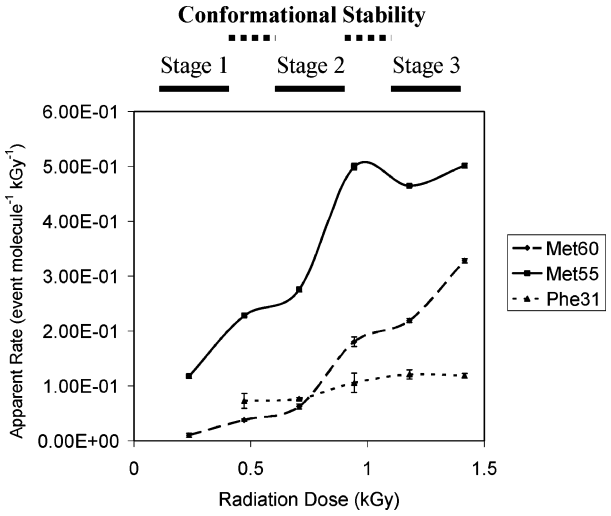

FIGURE 2: Summary of the three different categories of structural response to oxidative damage in Spo0F, as typified by the kinetics of oxidation of three oxidative damage targets. One category shows little increase in the kinetics of oxidation (e.g., Phe31); one category shows an intermediate increase in the kinetics of oxidation (e.g., Met60), and the third category shows the largest increase in the kinetics of oxidation (e.g., Met55). Error bars are shown for all data points and represent one standard deviation.

detected peptide are presented and discussed in full in the Supporting Information.

The kinetics of oxidation as a function of radiation dosage for each of the measured oxidation sites fell into three general categories of behavior (Figure 2). All peptides measured at lower radiation dosages (i.e., <0.472 kGy) exhibited a gradual increase in the rate of oxidation, representing a general destabilization of protein structure that does not have specific structural consequences. We have termed this phase of conformational change stage 1. This is followed by a period of stable kinetics of oxidation for almost all peptides measured from 0.472 to 0.708 kGy, indicating a region of conformational stability where additional oxidative damage does not cause marked destabilization of the protein. From 0.708 to 0.944 kGy, we begin to detect a differential structural response to an increased level of oxidative damage, indicative of a specific conformational change. Certain regions of the protein (exemplified in Figure 2 by Met55 and Met60) show a drastic increase in their rate of oxidation, indicating a dramatic increase in solvent accessibility (a 1.8-fold change with a 37 standard deviation difference and a 28.8-fold change with a 4 standard deviation difference, respectively). Other regions of the protein (exemplified in Figure 2 by Phe31) do not show a significant increase in the kinetics of oxidation over these radiation dosages (a 1.4-fold change, within two standard deviations of the 0.944 kGy data point), indicating that the conformational change is limited to specific regions of the protein. This period of conformational change is termed stage 2. Following this region of conformational change, almost all peptides exhibit no significant increase in the kinetics of oxidation between 0.944 and 1.180 kGy, again indicating a region of conformational stability in the face of additional oxidative damage.

Finally, with a radiation dose of 1.180−1.416 kGy, another differential conformational change is detected. Peptides that did not undergo a stage 2 conformational change (e.g., Phe31) also exhibit no change in the rate of oxidation for these dosages, indicating that these regions are still resistant to structural change due to oxidative damage. Some peptides that did experience the stage 2 conformational change also show no significant increase in the rate of oxidation from 1.180 to 1.416 kGy, as typified by Met55 in Figure 2. However, some of the peptides that experienced a stage 2 conformational change also show an increase in the rate of oxidation between these radiation dosages (e.g., Met60), indicating that these regions experience an additional increase in solvent accessibility. Again, the fact that most of the regions of Spo0F structure do not experience this conformational shift (as detected by an increase in the rate of oxidation) indicates that this is a specific conformational change due to oxidative damage, and not a general unfolding of the protein structure.

The sites of protein modification detected and their general response to oxidative damage are listed in Table 1. Attempts were made to determine the exact site(s) of modification for each peptide by MS/MS. In cases where the exact sites of modification were not able to be determined by MS/MS (due to a weak ion signal in the mass spectrum), any partial MS/MS data were considered with the primary sequence and structure of the native conformation of Spo0F, and the most

Table 1: Increase in the Rate of Oxidation as a Function of Radiation Dose[a]

		increase (*x*-fold)				
peptide	modified residue	stage 1	post-stage 1	stage 2	post-stage 2	stage 3
6−16	Tyr13[b]	ND	1.65	0	0	0
17−25	Leu18	4.88	1.30	2.26	0	1.24
26−45	(Tyr28, Phe31)	ND	0	1.38	0	0
46−56	Met55	1.93	1.21	1.81	0.932	1.08
57−67	Met60	3.69	1.63	2.89	1.21	1.50
71−77	Ile72	ND	ND	0	0	0
78−94	Met81, Met89[b]	ND	0.839	0	0.860	0.881
78−94	Asp88[c]	ND	3.23	6.44	1.43	1.18
95−104	(Phe102)	3.06	0	2.05	1.44	0
105−112	(Phe106)	ND	ND	ND	0	0
105−112	(Asp107, Asp109, Glu110)[c]	ND	ND	0	0	1.25
113−117	Asp113	2.03	0	1.49	0	0
118−122	(Tyr118, Pro120)	1.68	0	1.80	0.805	1.10

[a] Peptides with insufficient signal for oxidized peptides at a particular radiation dose are listed as not determined (ND). Amino acids listed in parentheses are presumed to be modified by the identity of the mass shift and the sequence of the peptide but have not been verified by MS/MS. [b] This oxidation target is fully exposed in the native structure and will not reflect unfolding events. [c] This oxidative damage is oxidative decarboxylation (loss of 30 Da).

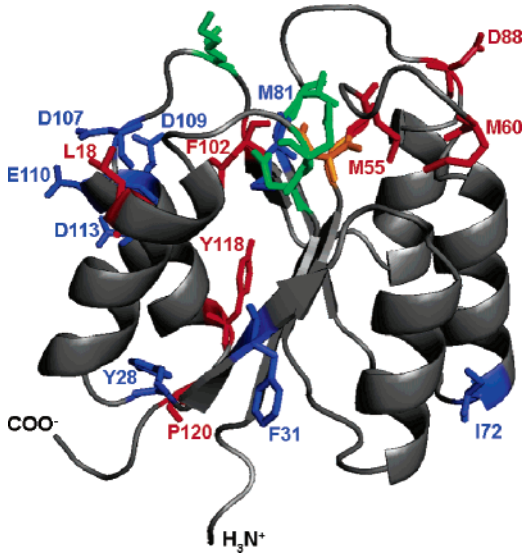

FIGURE 3: Increase in the kinetics of oxidation from 0.708 to 0.944 kGy plotted on the native structure of Spo0F. Regions that exhibited an at least 1.5-fold increase in the rate of oxidation from 0.708 to 0.944 kGy are colored red, while those that did not are colored blue. Residues that were oxidized but were not useful for probing structure from 0.708 to 0.944 kGy exposure are not shown. The phosphorylation site, Asp54, is colored orange, and the conserved residues, Asp10, Asp11, Thr82, and Lys104, are colored green.

likely site of modification was determined on the basis of the known chemical reactivity of the residue (*20*, *22*), the masses of their likely products (*21*, 22), and the average solvent accessibility of the potential targets in the native structure. As shown in Table 1, solvent accessibility data as a function of radiation dose were measured successfully for 13 different regions of the primary sequence in a single experiment, covering many different regions in the tertiary structure of Spo0F.

DISCUSSION

In this work, we have used oxidative surface mapping via mass spectrometry to independently and simultaneously monitor the solvent accessibility of more than 13 different oxidation targets in the sporulation-inducing protein Spo0F. The kinetics of formation for each oxidation product convey a unique story regarding the environment of that oxidation target. All oxidation targets exhibited a general increase in the rate of oxidation between 0.236 and 0.472 kGy, indicative of a general destabilization of the protein, followed by a period of conformational stability between 0.472 and 0.708 kGy, during which the rate of oxidation does not increase appreciably. However, between 0.708 and 0.944 kGy, the peptides begin to differ in their structural response to the process of oxidative damage. Analysis of these data allows for the elucidation of the specific conformational changes that Spo0F undergoes as a result of oxidative damage, which cannot be determined using circular dichroism.

Figure 3 shows the sites of oxidative damage and the general trend of their kinetics of oxidation from 0.708 to 0.944 kGy. Regions that experience this specific conformational change are grouped near the active site of the protein (except for residues near the C-terminus, which also experienced a modest increase in rate). Interestingly, residues that do not experience an increase in the rate of oxidation during this time are grouped away from the active site, in the portion of the protein structure responsible for maintaining the correct tertiary fold (except Met81, as discussed below). These data indicate that the conformational change that occurs between 0.708 and 0.944 kGy exposure involves the loops and the ends of the helices adjacent to the active site, while the structure of the protein distal from the active site (with the exception of the extreme C-terminal tail) remains undisturbed. Additionally, the fact that at least some regions of the active site become even more solvent-exposed at higher radiation dosages indicates that the conformational change between 0.708 and 0.944 kGy is not a transition to a wholly disordered state. This conformational change constitutes a specific and controlled unfolding event with a defined intermediate/transition state, rather than a global unraveling of the protein.

To lead to such a specific unfolding event, the conformational change experienced from 0.708 to 0.944 kGy exposure must be triggered by oxidative damage at a specific residue. Met60 is oxidized at a very low rate prior to this conformational change; however, after the conformational change, it is rapidly oxidized (Figure 2). Whatever the triggering oxidation event is, it must have occurred on a sufficient proportion of the protein to account for the increase that occurs from 0.708 to 0.944 kGy exposure. The average number of oxidations per peptide on Met60 at 0.708 kGy is 0.04436 (i.e., ~4% of Met60 is oxidized). The apparent rate of oxidation prior to the conformational change is ~0.06 event molecule^{-1} kGy^{-1}. If we extrapolate this (i.e., we assume no conformational change occurs), we expect that the average number of oxidations per peptide on Met60 at 0.944 kGy will be 0.05664 (i.e., ~6% of Met60 will be oxidized). What we observe is that ~17% is oxidized at 0.944 kGy. If we assume the most extreme case in which Met60 in every protein molecule in the new conformation oxidizes at 100% efficiency, we find that a minimum of 11% of the protein must be in the new conformation at 0.944 kGy. Examination of the amount of oxidation at each of the other sites shows that only Met55, Met81, and Met89 are modified to a sufficient extent to possibly be the trigger residue.

Another feature of the trigger oxidation event is that it *must precede* the conformational change; therefore, the kinetics of oxidation at that particular site will not reflect the conformational change itself. Examination of the kinetics of oxidation of Met55 (Figure 2) reveals that it does exhibit a marked increase in the rate of oxidation between 0.708 and 0.944 kGy exposure, eliminating it from contention as the possible trigger for the conformational change. Met81 and Met89 are on the same peptide; any analysis of the kinetics of oxidation will be confused by the fact that the rate reflects the combined rates of oxidation for both oxidation targets. MS/MS analysis of the singly oxidized and doubly oxidized peptide conclusively indicates that both residues are oxidized. The intensity of the signal suggests that the oxidation occurs at approximately the same rate for Met81 and Met89; however, oxidation of side chains may significantly alter the fragmentation characteristics in both a qualitative and quantitative manner (*26*), confounding any attempt to accurately measure the rate of oxidation at Met81 versus that of Met89 and forcing us to consider the rate of oxidation of the two sites together. Therefore, as the oxidation kinetics of this peptide fit the criteria for the

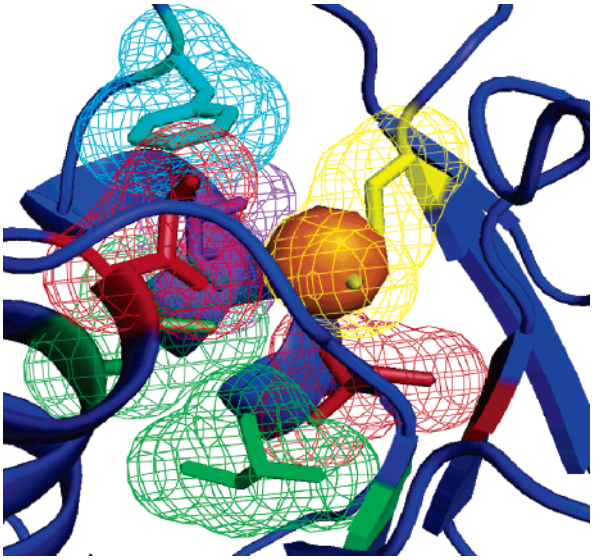

FIGURE 4: Detailed view of the Met81 binding pocket. Met81 is colored yellow, with the sulfur highlighted in orange. Ile8 is colored green, I15 red, Leu19 dark green, Leu52 maroon, Phe106 cyan, and Ile117 purple.

stage 2 trigger site, we cannot eliminate either Met81 or Met89 from consideration as the trigger for the conformational change. Examination of the environment of Met81 and Met89 in the structure of Spo0F is quite revealing. Met89 is almost fully exposed in the native state and is not tightly interacting with any other residue. On the other hand, Met81 serves as the core of a tightly packed hydrophobic pocket near the center of the active site. A closer view of this hydrophobic pocket is shown in Figure 4. Met81 serves as the center of this pocket, holding together residues from nearby loops and the ends of helices. Previous data also support the conclusion that Met89 is not structurally important, while Met81 is. Ala scanning mutagenesis showed that the Met81Ala mutant exhibited decreased enzymatic activity, while the Met89Ala mutant was fully functional (*27*). Therefore, we conclude that the conformational change between 0.708 and 0.944 kGy exposure is due to oxidation of Met81 to Met81═O.

Previous NMR data have shown that the loops around the active site are dynamic (*8*, *10*), which would allow transient access of the hydroxyl radical to Met81. Our data imply a model whereby Met81 is oxidized to the sulfoxide under relatively low radiation dosages (<0.944 kGy, considerably lower than the dosages required to unfold similarly sized globular proteins). The sulfoxide is bulkier than the undamaged methionine and considerably more polar. Met81═O flips out of the hydrophobic pocket and into the solvent, causing the structural elements that are held together by this hydrophobic pocket to undergo a conformational change and are rearranged to a different pseudostable conformation. Further oxidative damage of the protein can disrupt this structure as well (as indicated by increases in the kinetics of oxidation at dosages above 0.944 kGy, such as in Met60 of Figure 2), leading to further unfolding in this region, while the rest of the protein remains relatively unchanged. While this model is consistent with our data, as well as with previous mutation analysis data and NMR dynamics data, further study is required to fully validate and expand upon this model.

Spo0F is a member of the CheY superfamily of single-domain response regulators. Sequence analysis of the CheY domain shows that, while Met81 is conserved in a significant proportion of family members, it is often substituted for other hydrophobic amino acids (data not shown). One potential explanation for the conservation of methionine in position 81 in some family members but not in others is that a methionine in position 81 allows the protein to regulate its function in response to oxidative stress. Perhaps other CheY family members with methionine at position 81 act as oxidative stress sensors, modulating the cellular response due to specific oxidative damage in the presence of sufficient concentrations of reactive oxygen species. Significant study of the CheY superfamily must be carried out to test this hypothesis.

The data presented here represent the first report of the use of protein oxidative surface mapping to monitor the structural effects of oxidative damage. This technique represents a significant improvement over traditional techniques for studying heterogeneous protein damage products, as the conformation of many different sites can be determined simultaneously in one experiment using only the wild-type protein. The protein chemistry requires only the presence of water to function, and the modifications themselves are stable, allowing for any sample manipulations post-irradiation to be performed. The flexibility of the methodology allows for structural analysis of any protein with a known native structure under virtually any buffer conditions that are required (although certain buffer components that act as efficient radical scavengers would require increased radiation dosages to achieve similar effects). Membrane proteins could potentially be irradiated in a lipid bilayer, making this technique useful for studying the structural effects of oxidative damage on membrane proteins as well. As the proteins are enzymatically digested prior to analysis, there is no theoretical limit on the size of protein that can be analyzed, although limitations in resolution and dynamic range in mass spectrometry may limit the amount of information that can be gained from analysis of very large proteins. Experiments using stable isotopic labeling coupled with LC−MS are being carried out to attempt to increase the amount of information gained from such large proteins, as well as to attempt to gain information from proteins that do not currently have an unknown native structure.

ACKNOWLEDGMENT

Thanks to Erin Regel of the North Carolina State University Department of Molecular and Structural Biochemistry for expression and purification of the Spo0F protein utilized in this work.

SUPPORTING INFORMATION AVAILABLE

Plots and detailed analysis of the circular dichroism data as well as the kinetics of oxidation for all detected oxidation sites. This material is available free of charge via the Internet at http://pubs.acs.org.

REFERENCES

1. Storz, G., and Zheng, M. (2000) Oxidative Stress, in *Bacterial Stress Responses* (Strorz, G., and Hengge-Aronis, R., Eds.) pp 47−59, ASM Press, Washington, DC.

2. Sahoo, S., Rao, K. K., Suresh, A. K., and Suraishkumar, G. K. (2004) Intracellular reactive oxygen species mediate suppression of sporulation in *Bacillus subtilis* under shear stress, *Biotechnol. Bioeng. 87*, 81−9.
3. Errington, J. (2003) Regulation of endospore formation in *Bacillus subtilis*, *Nat. Rev. Microbiol. 1*, 117−26.
4. Dowds, B. C., Murphy, P., McConnell, D. J., and Devine, K. M. (1987) Relationship among oxidative stress, growth cycle, and sporulation in *Bacillus subtilis*, *J. Bacteriol. 169*, 5771−5.
5. Yasbin, R. E., Cheo, D., and Bol, D. (1993) DNA Repair Systems, in *Bacillus subtilis and Other Gram-Positive Bacteria* (Sonenshein, A. L., Hoch, J. A., and Losick, R., Eds.) pp 529−37, ASM Press, Washington, DC.
6. Burbulys, D., Trach, K. A., and Hoch, J. A. (1991) Initiation of sporulation in *B. subtilis* is controlled by a multicomponent phosphorelay, *Cell 64*, 545−52.
7. Sonenshein, A. L. (2000) Bacterial Sporulation: A Response to Environmental Signals, in *Bacterial Stress Responses* (Storz, G., and Hengge-Aronis, R., Eds.) pp 199−215, ASM Press, Washington, DC.
8. Feher, V. A., and Cavanagh, J. (1999) Millisecond-timescale motions contribute to the function of the bacterial response regulator protein Spo0F, *Nature 400*, 289−93.
9. Feher, V. A., Zapf, J. W., Hoch, J. A., Dahlquist, F. W., Whiteley, J. M., and Cavanagh, J. (1995) ^{1}H, ^{15}N, and ^{13}C backbone chemical shift assignments, secondary structure, and magnesium-binding characteristics of the *Bacillus subtilis* response regulator, Spo0F, determined by heteronuclear high-resolution NMR, *Protein Sci. 4*, 1801−14.
10. Feher, V. A., Zapf, J. W., Hoch, J. A., Whiteley, J. M., McIntosh, L. P., Rance, M., Skelton, N. J., Dahlquist, F. W., and Cavanagh, J. (1997) High-resolution NMR structure and backbone dynamics of the *Bacillus subtilis* response regulator, Spo0F: Implications for phosphorylation and molecular recognition, *Biochemistry 36*, 10015−25.
11. Tzeng, Y. L., and Hoch, J. A. (1997) Molecular recognition in signal transduction: The interaction surfaces of the Spo0F response regulator with its cognate phosphorelay proteins revealed by alanine scanning mutagenesis, *J. Mol. Biol. 272*, 200−12.
12. Tzeng, Y. L., Feher, V. A., Cavanagh, J., Perego, M., and Hoch, J. A. (1998) Characterization of interactions between a two-component response regulator, Spo0F, and its phosphatase, RapB, *Biochemistry 37*, 16538−45.
13. Hoch, J. A., and Varughese, K. I. (2001) Keeping signals straight in phosphorelay signal transduction, *J. Bacteriol. 183*, 4941−9.
14. Chance, M. R. (2001) Unfolding of apomyoglobin examined by synchrotron footprinting, *Biochem. Biophys. Res. Commun. 287*, 614−21.
15. Sharp, J. S., Becker, J. M., and Hettich, R. L. (2004) Analysis of protein solvent accessible surfaces by photochemical oxidation and mass spectrometry, *Anal. Chem. 76*, 672−83.
16. Sharp, J. S., Becker, J. M., and Hettich, R. L. (2003) Protein surface mapping by chemical oxidation: Structural analysis by mass spectrometry, *Anal. Biochem. 313*, 216−25.
17. Hambly, D. M., and Gross, M. L. (2005) Laser flash photolysis of hydrogen peroxide to oxidize protein solvent-accessible residues on the microsecond time scale, *J. Am. Soc. Mass Spectrom. 16*, 2057−63.
18. Goldsmith, S. C., Guan, J. Q., Almo, S., and Chance, M. (2001) Synchrotron protein footprinting: A technique to investigate protein−protein interactions, *J. Biomol. Struct. Dyn. 19*, 405−18.
19. Maleknia, S. D., Ralston, C. Y., Brenowitz, M. D., Downard, K. M., and Chance, M. R. (2001) Determination of macromolecular folding and structure by synchrotron X-ray radiolysis techniques, *Anal. Biochem. 289*, 103−15.
20. Buxton, G. V., Greenstock, C. L., Helman, W. P., and Ross, A. B. (1988) Critical-Review of Rate Constants for Reactions of Hydrated Electrons, Hydrogen-Atoms and Hydroxyl Radicals (Oh/$^{\bullet}O^{-}$) in Aqueous Solution, *J. Phys. Chem. Ref. Data 17*, 513−886.
21. Garrison, W. M. (1987) Reaction Mechanisms in the Radiolysis of Peptides, Polypeptides, and Proteins, *Chem. Rev. 87*, 381−98.
22. Xu, G., and Chance, M. R. (2005) Radiolytic modification and reactivity of amino acid residues serving as structural probes for protein footprinting, *Anal. Chem. 77*, 4549−55.
23. Zapf, J. W., Hoch, J. A., and Whiteley, J. M. (1996) A phosphotransferase activity of the *Bacillus subtilis* sporulation protein Spo0F that employs phosphoramidate substrates, *Biochemistry 35*, 2926−33.
24. Xu, G., Kiselar, J., He, Q., and Chance, M. R. (2005) Secondary reactions and strategies to improve quantitative protein footprinting, *Anal. Chem. 77*, 3029−37.
25. Madhusudan, Zapf, J., Whiteley, J. M., Hoch, J. A., Xuong, N. H., and Varughese, K. I. (1996) Crystal structure of a phosphatase-resistant mutant of sporulation response regulator Spo0F from *Bacillus subtilis*, *Structure 4*, 679−90.
26. Grunert, T., Pock, K., Buchacher, A., and Allmaier, G. (2003) Selective solid-phase isolation of methionine-containing peptides and subsequent matrix-assisted laser desorption/ionisation mass spectrometric detection of methionine- and of methionine-sulfoxide-containing peptides, *Rapid Commun. Mass Spectrom. 17*, 1815−24.
27. Jiang, M., Tzeng, Y. L., Feher, V. A., Perego, M., and Hoch, J. A. (1999) Alanine mutants of the Spo0F response regulator modifying specificity for sensor kinases in sporulation initiation, *Mol. Microbiol. 33*, 389−95.

BI060470R